Supplemental Figures and Extended Data for: Large-scale neural recordings with single-cell resolution in human cortex using high-density Neuropixels probes

AUTHORS

Angelique C. Paulk[1], Yoav Kfir[2], Arjun Khanna[2], Martina Mustroph[2], Eric M. Trautmann[3], Dan J. Soper[1], Sergey D. Stavisky[4], Marleen Welkenhuysen[5], Barundeb Dutta[5], Krishna V. Shenoy[6], Leigh R. Hochberg[1,7], R. Mark Richardson[2], Ziv M. Williams[2]*, and Sydney S. Cash[1]*

AUTHOR INFORMATION

[1]Department of Neurology, Harvard Medical School, Boston, MA, USA; Center for Neurotechnology and Neurorecovery, Department of Neurology, Massachusetts General Hospital, Boston, MA, USA.

[2]Dept. of Neurosurgery, Harvard Medical School and Massachusetts General Hospital, Boston, MA, USA.

[3]Zuckerman Institute, Columbia University, New York, NY; Department of Electrical Engineering, Stanford University, Stanford, CA, USA; Wu Tsai Neurosciences Institute, Bio-X Program, Stanford University, Stanford, CA, USA; Howard Hughes Medical Institute at Stanford University, Stanford, CA, USA.

[4]Department of Neurosurgery, Stanford University, Stanford, CA, USA; Department of Electrical Engineering, Stanford University, Stanford, CA, USA; Wu Tsai Neurosciences Institute, Bio-X Program, Stanford University, Stanford, CA, USA.

[5]IMEC, Leuven, Belgium.

[6]Department of Electrical Engineering, Stanford University, Stanford, CA, USA; Department of Bioengineering, Stanford University, Stanford, CA, USA; Department of Neurobiology, Stanford University, Stanford, CA, USA; Howard Hughes Medical Institute at Stanford University, Stanford, CA, USA; Wu Tsai Neurosciences Institute, Bio-X Program, Stanford University, Stanford, CA, USA.

[7]VA RR&D Center for Neurorestoration and Neurotechnology, Rehabilitation R&D Service, Providence VA Medical Center, Providence, RI, USA; School of Engineering and Carney Institute for Brain Science, Brown University, Providence, RI, USA.

* Co-senior authors

CORRESPONDENCE

Angelique C. Paulk, Sydney S. Cash and Ziv M. Williams

Mail: 55 Fruit St. Boston, MA 02114

Email: apaulk@mgh.harvard.edu, scash@mgh.harvard.edu, zwilliams@mgh.harvard.edu

Number of Figures: 5

Number of Tables: 0

Number of Extended Data Figures and tables: 6

Number of Supplementary Videos: 0

METHODS (COMPLETE ONLINE VERSION).

Patients & clinical/research electrode placement

All patients voluntarily participated after informed consent according to NIH guidelines as monitored by the Partners Institutional Review Board (IRB) Massachusetts General Hospital (MGH). Participants were informed that participation in the experiment would not alter their clinical treatment in any way, and that they could withdraw at any time without jeopardizing their clinical care. Recordings in the operating room were acquired with 9 participants (mean= 59 years old, ranging from 34 to 75; 7 female; **Supplemental Table 1**) who were already scheduled for a craniotomy for concurrent clinical intraoperative neurophysiological monitoring or testing for mapping motor, language, and sensory regions and removal of tissue as a result of tumor or epilepsy or undergo intra-operative neurophysiology as part of their planned deep brain stimulator (DBS) placement [1–4]. Prior to inserting the Neuropixels probe, a small superficial incision in the pia was done using an arachnoid surgical knife. The Neuropixels probe was inserted through this incision. Recordings were referenced to sterile ground and recording reference needle electrodes (Medtronic) placed in nearby muscle tissue (often scalp) as deemed safe by the neurosurgical team though a series of tests ground and reference tests were performed to identify the ideal combinations of ground and reference options, listed below (**Supplemental Table 1**).

Following the surgery, the preoperative T1-weighted MRI was used to generate a 3D surface brain map using FreeSurfer scripts [5–7] (http://surfer.nmr.mgh.harvard.edu). Images obtained during surgery and locations as indicated using Brainlab (Brainlab, Inc.) captured during the surgery were aligned to the 3D reconstructions using Blender software (https://www.blender.org/) and MMVT [7–9]. The method involved projecting the surgical image onto the patient's reconstructed brain using Blender and then placing a 3D model of the Neuropixels probe on that location similar to other coregistration approaches [4,7,8,10]. Angles were calculated from photographs taken during the surgery as well as trajectories limited by the location and angle of the burr hole for DBS surgery.

Neuropixels recordings, data collection & analysis

Neuropixels probes (NP v 1.0, version S, IMEC) sterilized with Ethylene Oxide (BioSeal) were connected to a 3B2 IMEC headstage wrapped in a sterile plastic bag and sealed using TegaDerm (3M) to keep the field sterile. Neuropixels probes (NP v 1.0-S, IMEC) include an electrode shank (width: 70µm, length: 10 mm, thickness: 100µm) of 960 total sites laid out in a checkerboard pattern with contacts at ~18 µm site to site distances (16 µm (column), 20 µm

(row); [11]). Handling of the electrodes and the headstage from outside the sterile bag was all performed in sterile conditions in the operating room. The headstage was connected via a multiplexed cable to a PXIe acquisition module card (IMEC), installed into a PXIe Chassis (PXIe-1071 chassis, National Instruments). All Neuropixels recordings were performed using SpikeGLX (http://billkarsh.github.io/SpikeGLX/) on a computer connected to the PXIe acquisition module recording the action potential band (AP, band-pass filtered from 0.3-10 kHz) sampled at 30 kHz and a local field potential band (LFP, band-pass filtered from 0.5-500 Hz), sampled at 2.5 kHz [11–13]. Since these Neuropixels probes enable 384 recording channels which can then be used to address 960 electrodes across the probe shank, we tested different electrode maps which allowed us to record different portions of the probe. One map allowed for recording the lower portion of the probe (the most distal channels). A second map allowed for recording two rows along the entire length of the electrode. This map was used to identify the depth of the electrode in the cortex and we switched to the distal tip map (short map) for the main recording. A final map allowed for recording in a series of tetrode locations, skipping rows to distribute recordings along the entire length of the probe.

Synchronization was performed through two different approaches. TTL triggers via a parallel port produced either during a task via MATLAB or custom code from a separate computer were sent to both the National Instruments and IMEC recording systems, via a parallel port system. In addition, we used the TTL output to send the synchronization trigger via the SMA input to the IMEC PXIe acquisition module card to allow for added synchronizing triggers which were also recorded on an additional breakout analog and digital input/output board (BNC-2110, National Instruments) connected via a PXIe board (PXIe-6341 module, National Instruments). The TTL triggers were produced either during a task via MATLAB or custom code on the task computer.

Recording challenges and lessons learned

Five main challenges were faced when performing these recordings: 1) sterilization and maintaining a sterile field and conditions; 2) electrode fracture and disconnects; 3) decreasing noise in the recordings through referencing; 4) external sources of noise; 5) mechanical stabilization (**Fig. 1**; **Supplemental Fig. 1**).

Sterilization and maintaining a sterile field

To ensure we could use the Neuropixels probes in the OR, we worked with BioSeal (Placentia, CA) and sent them a sample of 25 Neuropixels probes. BioSeal took the samples through a validation process to determine that ethylene oxide (EtO) could be used to sterilize

the Neuropixels probes. We also tested whether working Neuropixels probes were operational before and after sterilization. An important part of the process was identifying safe sterile packaging for sterilization and transport. We found we could place the probes sideways inside a slightly modified EtO-safe sterile container (SteriBest Trays, Sterilization Instrument Tray, Instrument Tray Sizes (inches):Base, Lid, Mat 6x2.5x.75], item#A-CP614, from Duraline Biosystem; **Fig. 1a**; **Supplemental Fig. 1g**; **Supplemental Table 1**). When received the boxes, we clipped protruding silicone nubs in an area of 3 cm x 3 cm on one side of the box as well as a few silicone nubs on the other end of the box. We found that we could package and safely ship and handle the Neuropixel probe cross-country by weaving the Neuropixels ribbon cable around the vertical silicone nubs in the sterilization containers with the Neuropixels probe and headstage perpendicular to the base of the box. We performed several tests to demonstrate the probe consistently survived this shipment approach, including before and after sterilization. Before shipping for sterilization, we soldered on a 10 cm long male touchproof cable (the white cable in Fig. 1a, b and d) to the reference side of the Neuropixels probe. In addition, we labelled the lid of the box to track individual probes. The validation of 25 probes performed by BioSeal was done with the Neuropixels probes in this configuration and with this specific SteriBest Tray packaging (including the added touchproof connection cable). Once shipped to Bioseal packed in bubble wrap, the company would return the probes in their sterilization boxes sealed in approved packaging. We have found this approach kept the electrodes intact and tracked throughout transport and sterilization.

Electrode fractures and disconnects

We had instances of electrode fracture (N=2), both of which were with the thinner Neuropixels 1.0 probes (thickness: 25µm, width: 70µm, length: 10 mm). We then switched to a thicker custom Neuropixels 1.0-S probe (thickness: 100µm width: 70 µm, length: 10 mm) for the remaining recordings and, of the 7 uses of thick probes, we only had one instance of electrode fracture. In each instance, we documented whether the probes were intact afterward both via the SpikeGLX software and through thorough photograph documentation. In the three probes which were fractured, we were able to photograph the pieces to reconstruct the entire probe do validate probe recovery. In the remaining probes, the photographs after the case confirmed the electrodes were fully intact after the case. In addition, in the intact probes after the case, software check via SpikeGLX involved a hardware check indicating the probes were intact and fully functioning.

Decreasing noise using referencing and grounding

Even though we had tested the Neuropixels probe as well as had considerable experience in using Neuropixels in NHPs which informed how we built our electrophysiological system [13], we found moving the Neuropixels recordings into the human OR was made much more difficult with considerable added noise compared to any of the other testing settings. In the first four tests, we followed the original recommendations to tie the reference to the ground on the Neuropixels probe which degraded the signal considerably in the OR (**Supplemental Fig. 1a**). The signal was substantially improved by separating the ground and reference on the Neuropixels probe, with a single Medtronic sterile wire connected to the reference placed in the scalp and a separate wire attached to the ground and also placed in the scalp as deemed safe by the neurosurgical team. Improving the signal also involved tying the patient ground to the recording ground the patient to the recording via a BOVIE pad (Clearwater, FL) connected to the grounding BNC on the NIDAQ board used for the Neuropixels system. Placing the grounding lead into saline or CSF degraded the signal by saturating the LFP and increasing noise in the system.

External sources of noise

Changing the reference from the external reference in the software (using SpikeGLX) to the internal reference also increased noise significantly (**Supplemental Fig. 1c**). We also discovered an external source of noise was the wall-powered anesthesia IV pump (as is commonly used during patient transport) which, when unplugged and operating on battery, would decrease the physiological noise. Finally, we did a series of tests to determine if other signals added sources of noise and we did not find an effect of the BOVIE cautery machine, the ROSA robot, the lights or other machines in the room.

Mechanical stabilization

Two separate stabilization approaches were tested. One approach involved the patients receiving DBS implantations at MGH, who normally also undergo standardized micro-electrode recording to optimize anatomical targeting [1,14], Neuropixels probes were inserted in the same locations as the microelectrodes that traverse the dorsal lateral surface of the prefrontal cortex on the way to the target nucleus, offering a brief chance to study neuronal dynamics in the dlPFC and not perturbing the planned operative approach nor alter clinical care [1–3,14–16]. Three cannulae were placed in a manipulator (AlphaOmega Engineering, Nazareth, Israel) and the Neuropixels probe was attached to the cannulae using SteriStrips (3M™ Steri-Strip™ Reinforced Adhesive Skin Closures). The manipulator was attached to the ROSA ONE® Brain (Zimmer Biomet) arm. The Neuropixels probe was put over the burr hole by the ROSA robot arm. ROSA was then used to move the probe insert the probe using fine millimeter steps, with

some adjustment possible using the AlphaOmega micromanipulator.The second approach involved securing the Neuropixels probe to a sterile syringe which was then held by a 3-axis micromanipulator built for Utah array placement (BlackRock, Salt Lake City, UT) which was attached to a Greenberg retractor. The Neuropixels probe was in place and lowered using the micromanipulator.

Compensation for tissue movement and electrode alignment through time

We found clear evidence of vertical tissue movement relative to the Neuropixels probe in the local field potential (LFP) recordings (**Supplemental Fig. 2**). To confirm that this was due to movement of the tissue as well as effects of heartbeat, we aligned the movement artifact to the heartbeat in time (this was possible thanks to audio tracking of the EKG in 2 participants' cases). We found the movement roughly matched this tracking. To confirm that the manual tracking could match the movement of the brain relative to the electrode, we performed tissue-level tracking of the video recordings of the case and found we could align the filmed movement of the brain pumping relative to the electrode, which was well visualized in the LFP band across channels as tracked through time (**Supplemental Fig. 2b**). We tested several approaches to address this movement and correct for the alignment, including the Kilosort 3.0 drift adjustments and estimation (https://github.com/MouseLand/Kilosort) and spike time-informed alignment approaches (https://github.com/evarol/NeuropixelsRegistration). We chose to use the LFP-informed manual tracking as it was better-resolved in the time domain since the dynamic range of LFP allowed for per time step (0.0004 sec) alignment and interpolation. In contrast, the automatic approach depended on firing rate and arrival of spikes, which were sparse (**Fig. 1e-f**).

Manual tracking of movement using LFP signals

The signal was first extracted from the binary files into local field potential (LFP, <500 Hz filtered data, sampled at 2500 Hz) and action potential (AP, >500 Hz filtered data, sampled at 30000 Hz) from SpikeGLX using MATLAB and available preprocessing code (https://billkarsh.github.io/SpikeGLX/). We inspected the data visually as well as examined the timeline of the recording to reject noisy time ranges (such as during insertion.) We then further examined the voltage deflections in the LFP for a prominent, bounded deflection in the voltage where we observed the voltage values shifting in unison(**Supplemental Figure 2**) which was consistently present throughout the recording (blue or red bands in **Supplemental Figure 2**). We attempted to use a number of algorithms to detect these shifts, but the multiple changes present (heartrate, slow and mid-range drifting, and other shifts) were not effectively tracked by these algorithms. Instead, to capture the displacement in the movement bands, we imported the

LFP voltage as an .stl file from MATLAB into Blender (https://www.blender.org/), a three dimensional animation program which allowed for easier manual tracing compared to MATLAB. Using the surface voltage and the Grease Pencil feature, we traced the shifting band of negatively deflecting LFP throughout the recording at a resolution of 500 Hz. The line produced then was exported as a .csv file and imported into MATLAB, where it was compared with the LFP at higher resolution to check whether the manual tracing matched the LFP displacement (**Supplemental Figure 2a**). This traced line information was upsampled to 2500 Hz to match the sampling frequency of the LFP channels (interp1, 'makima').

Preprocessing AP recordings

Once we had the LFP baseline to track probe movement through time, we then applied analyses to the AP sampled band. To account for differences in the channels before aligning the data (as channels can have differences in impedance), we first detrended data (which removes best fitted line to each channel), calculated the median, and subtracted it from all channels. We then normalized the voltage signal across channels by multiplying each channel's voltage time series by a normalization factor where *Normalized data = Channel signal * (1/std) * 600*. In this case, the *std* was the standard deviation of channel data without outliers, particularly epochs which were relatively quiet. We defined outliers as elements which were more than 1.5 interquartile ranges above the upper quartile or below the lower quartile of the distribution of voltage signals. Finally, we chose the value of 600 in the normalization to allow us to scale the data up to an int16 format for improved data resolution.

Alignment and interpolation of AP channels for manual registration

To then re-align the AP channel data so as to offset the movement artifact, we upsampled the traced line to 30KHz to match the AP sampling rate (interp1, 'makima'). We then, for each time bin, applied a spatial interpolation between channels vertically in two columns of the Neuropixels recording, resulting in a vertical spatial resolution of 1um. (**Supplemental Figure 2**). These steps resulted in a large, high resolution interpolated matrix that we could then follow through time. This let us compensate for the movement effects by resampling the voltage in space (**Supplemental Figure 2**) based on the manually registered movement trajectory described in "Manual Tracking of Movement using LFP signals".

Specifically, for each time bin, we shifted the vertical channels vector up or down according the upsampled traced line, resulting in >450 'virtual channels' that each contained voltage information putatively from a specific brain location. Finally, since the virtual channels on

both ends (top and bottom of the shank) contained only partial data (due to brain movement relative to the electrode), we selected a subset of 384 virtual channels that contained the most continuous information throughout the recording (and did not shift channels into the edge), which could be inferred from the average channel offset.

Unit isolation and clustering

Single unit sorting was performed using Kilosort 3.0 [17] (https://github.com/MouseLand/Kilosort) as well as Phy (https://github.com/cortex-lab/phy) and then manually curated using in-house MATLAB code to visually inspect the template as well as the waveforms assigned to each cluster. The Kilosort 3.0 parameters included: Nblocks = 0 – as no additional registration was needed according to spiking activity after the manual registration; Threshold [10, 11] to be more strict in our detections (initial values were [9,9] which resulted in ~800 units for Pt. 02). Clusters were merged in Phy if the templates were similar between clusters, the spatial spread of waveforms were highly similar and overlapping, and cross-correlations of the event times indicated high levels of correlation. To further process and shift each individual waveform to correct for Kilosort3 misalignment, we also calculated the cross correlation of individual waveforms with the cluster template and adjusted waveforms according to location of maximal voltage value per waveform in the sampled time.

Waveform feature analyses and classification

Clusters were then separated into single units and multi-unit activity (MUA). Units were classified as MUA if there was a mixture of distinct waveforms (examined in Phy) as well as a complicated (and abnormal) autocorrelogram. For all units, we then measured the spike duration, halfwidth, peak-trough ratio, repolarization slope, recovery slope, and amplitude measures (**Fig. 2**; adapted from [12]; https://github.com/jiaxx/waveform_classification). Further, we applied the spatial spread and velocity measures to each cluster to identify whether we could observe evidence for backpropagating action potentials or other unique spatial dynamics (**Fig. 2**; adapted from [12]).

We used three different classification approaches to group the units. First, using a standard approach, units were grouped into regular spiking (RS), fast spiking (FS), positive spikes (PS) classifications based on the spike waveform duration (valley-to-peak) of the largest peak across channels per unit [18–23]. The ranges for each classification were as follows: negative going peaks included FS (duration <0.3 ms) and RS (duration>0.3 ms) and positive spikes (PS). Second, we applied principal components analyses on the first six channels per unit and

clustered these average waveforms using k-means clustering (squared Euclidean distance, 1000 replicates, 1000 maximum iterations) into 7 clusters based on the separability of the clusters (using silhouette) and how clean the resulting clusters were. Finally, we used a novel non-linear method, WaveMAP, which took into account the spatial and temporal waveform characteristics while separating out differences in the waveforms [24]. WaveMAP includes a combination of dimensionality reduction with Universal Manifold Approximation and Projection (UMAP) combined with Louvain clustering to identify clusters in the data set [24]. We then compared the waveform features across these different classifications.

Local field potential analyses

Custom MATLAB code (version R2020a) in combination with open source code from the Fieldtrip toolbox ([25]; http://www.fieldtriptoolbox.org/).

Burst suppression ratio measurement

The burst suppression ratio (BSR) was computed using an automated method [26,27] (https://github.com/drasros/bs_detector_icueeg). After averaging the LFP across all channels, this method then labels each time sample as either burst or suppression. Briefly, the method uses the previous data with each channel and applies the following equations:

$$\mu t = \beta\, \mu t\text{-}1 + (1-\beta)\, xt$$

$$\sigma t2 = \beta\, \sigma t\text{-}12 + (1-\beta)\, (xt - \mu t)2$$

$$zt = \delta[\sigma t2 < \theta]$$

Where xt is the value of the normalized signal of one channel at time t, μt and σt2 are current values of the recursively estimated local mean and variance, respectively. Finally, zt is an indicator function that labels each data point as either a burst (0) or suppression (1). The value of β determines the balance between the effect of recent and past data set based on previously trained data [26]. The classification threshold θ (i.e., the value above which a data point should be classified as burst) was adjusted to evaluate our dataset visually with values of θ = 50, 100, 150, and 200 and was informed by the input from two experts who reviewed selected intervals to identify burst and suppression using each possible theta value. The value of θ = 200 was selected to reliably identify burst and suppression induced by general anesthesia. The burst suppression ratio for each recording in an anesthetized patient (N=2) was evaluated as the proportion of suppression-labeled samples in a moving window (1 s duration, no overlap).

Inter-ictal epileptiform discharges

In one case, the Neuropixels electrode was inserted into the lateral temporal lobe before tissue resection for epilepsy. As we could identify interictal epileptiform discharges (IIDs) in the LFP, we applied both an automatic and a visual detection approach to verify the timing and location of the IIDs in the Neuropixels recording. For automatic detection, we averaged the LFP across channels and applied the algorithm of [28], version v21, default settings except -h at 60 and -k1 at 7 to increase the threshold for detection; http://isarg.fel.cvut.cz), which adaptively models distributions of signal envelopes to discriminate IIDs from LFP [28]. In addition, a trained and experienced epileptologist (SSC) examined the average LFPs and confirmed the timing of the detected IIDs. This two-step process was necessary as the burst suppression from the anesthesia produced waveforms which could obscure the IIDs. For several analyses, the single unit spike times were then aligned relative to the peaks of the IIDs.

Statistical analysis

All statistical comparisons were performed using non-parametric measures, so we did not test for normality. Multiple comparisons tests were performed using the Kruskal–Wallis test for non-equivalence of multiple medians followed post hoc Tukey-Kramer method to identify statistically separable groups. For comparisons between individual medians, we used the Wilcoxon rank-sum test (two-sided). We corrected by adjusting the target p-value (0.05) with a Bonferroni correction for the number of comparisons being done.

Data availability

The majority of the data that support the findings of this study are available from the corresponding author upon reasonable request, though a subset of data will be available for download at Dryad (https://datadryad.org/stash) upon publication.

Code availability

Open source acquisition software, SpikeGLX (http://billkarsh.github.io/SpikeGLX/) and record the neural data. Single unit sorting was performed using Kilosort 3.0 [17] (https://github.com/MouseLand/Kilosort) as well as Phy (https://github.com/cortex-lab/phy) Custom Matlab code (version R2020a) and python code in combination with open source code from the Fieldtrip toolbox (http://www.fieldtriptoolbox.org/) was used for the majority of the analyses with some code involving manual alignment available on Github (https://github.com/Center-For-Neurotechnology/CorticalNeuropixelProcessingPipeline). The burst suppression ratio (BSR) was computed using an automated method [26,27]

(https://github.com/drasros/bs_detector_icueeg). Reconstruction of electrode locations and the manual tracing was done using the open source, free software Blender (https://www.blender.org/).

METHODS REFERENCES

1. Patel, S. R. *et al.* Studying task-related activity of individual neurons in the human brain. *Nat. Protoc.* **8**, 949–957 (2013).
2. Jamali, M. *et al.* Dorsolateral prefrontal neurons mediate subjective decisions and their variation in humans. *Nat. Neurosci.* **22**, 1010–1020 (2019).
3. Jamali, M. *et al.* Single-neuronal predictions of others' beliefs in humans. *Nature* **591**, 610–614 (2021).
4. Paulk, A. C. *et al.* Microscale Physiological Events on the Human Cortical Surface. *Cereb. Cortex* (2021) doi:10.1093/cercor/bhab040.
5. Reuter, M., Rosas, H. D. & Fischl, B. Highly Accurate Inverse Consistent Registration: A Robust Approach. *NeuroImage* **53**, 1181–1196 (2010).
6. Reuter, M., Schmansky, N. J., Rosas, H. D. & Fischl, B. Within-Subject Template Estimation for Unbiased Longitudinal Image Analysis. *NeuroImage* **61**, 1402–1418 (2012).
7. Dykstra, A. R. *et al.* Individualized localization and cortical surface-based registration of intracranial electrodes. *Neuroimage* **59**, 3563–3570 (2012).
8. Holmes, C. J. *et al.* Enhancement of MR Images Using Registration for Signal Averaging. *J. Comput. Assist. Tomogr.* **22**, 324–333 (1998).
9. Felsenstein, O. & Peled, N. *MMVT – Multi-Modality Visualization Tool*. *GitHub Repository* (2017). doi:10.5281/zenodo.438343.
10. Postelnicu, G., Zöllei, L. & Fischl, B. Combined Volumetric and Surface Registration. *IEEE Trans. Med. Imaging* **28**, 508–522 (2009).
11. Jun, J. J. *et al.* Fully integrated silicon probes for high-density recording of neural activity. *Nature* **551**, 232–236 (2017).

12. Jia, X. *et al.* High-density extracellular probes reveal dendritic backpropagation and facilitate neuron classification. *J. Neurophysiol.* **121**, 1831–1847 (2019).
13. Trautmann, E. M. *et al.* Accurate Estimation of Neural Population Dynamics without Spike Sorting. *Neuron* **103**, 292-308.e4 (2019).
14. Amirnovin, R., Williams, Z. M., Cosgrove, G. R. & Eskandar, E. N. Experience with microelectrode guided subthalamic nucleus deep brain stimulation. *Neurosurgery* **58**, ONS96-102 (2006).
15. Sheth, S. a *et al.* Human dorsal anterior cingulate cortex neurons mediate ongoing behavioural adaptation. *Nature* **488**, 218–21 (2012).
16. Mian, M. K. *et al.* Encoding of rules by neurons in the human dorsolateral prefrontal cortex. *Cereb. Cortex* **24**, 807–816 (2014).
17. Pachitariu, M., Steinmetz, N., Kadir, S., Carandini, M. & Harris, K. Fast and accurate spike sorting of high-channel count probes with KiloSort. *Adv. Neural Inf. Process. Syst.* **2016**, 1–9 (2016).
18. McCormick, D. A., Connors, B. W., Lighthall, J. W. & Prince, D. A. Comparative electrophysiology of pyramidal and sparsely spiny stellate neurons of the neocortex. *J. Neurophysiol.* **54**, 782–806 (1985).
19. Bartho, P. *et al.* Characterization of Neocortical Principal Cells and Interneurons by Network Interactions and Extracellular Features. *J. Neurophysiol.* **92**, 600–608 (2004).
20. Mitchell, J. F., Sundberg, K. A. & Reynolds, J. H. Differential Attention-Dependent Response Modulation across Cell Classes in Macaque Visual Area V4. *Neuron* **55**, 131–141 (2007).
21. Snyder, A. C., Morais, M. J. & Smith, M. A. Dynamics of excitatory and inhibitory networks are differentially altered by selective attention. *J. Neurophysiol.* **116**, 1807–1820 (2016).
22. Dickey, C. W. *et al.* Travelling spindles create necessary conditions for spike-timing-dependent plasticity in humans. *Nat. Commun.* **12**, 1027 (2021).

23. Sun, S. H. *et al.* Analysis of extracellular spike waveforms and associated receptive fields of neurons in cat primary visual cortex. *J. Physiol.* **8**, 2211–2238 (2021).
24. Lee, E. K. *et al.* Non-linear Dimensionality Reduction on Extracellular Waveforms Reveals Physiological, Functional, and Laminar Diversity in Premotor Cortex. *bioRxiv* 2021.02.07.430135 (2021).
25. Oostenveld, R., Fries, P., Maris, E. & Schoffelen, J.-M. FieldTrip: Open source software for advanced analysis of MEG, EEG, and invasive electrophysiological data. *Comput. Intell. Neurosci.* **2011**, 156869 (2011).
26. Westover, M. B. *et al.* Real-time segmentation of burst suppression patterns in critical care EEG monitoring. *J. Neurosci. Methods* **219**, 131–141 (2013).
27. Salami, P., Borzello, M., Kramer, M. A., Westover, M. B. & Cash, S. S. Quantification of seizure termination patterns reveals limited pathways to seizure end. *medRxiv* (2021) doi:10.1101/2021.03.03.21252789.
28. Janca, R. *et al.* Detection of Interictal Epileptiform Discharges Using Signal Envelope Distribution Modelling: Application to Epileptic and Non-Epileptic Intracranial Recordings. *Brain Topogr.* **28**, 172–183 (2015).

Extended Data Figures

Supplemental Table 1. Distribution and numbers of cases and results as well as reasons for data exclusion and information per participant and recording

Participant	Procedure	Location	Type	Recording and number of units	Reason for exclusion of data
	left anterior frontal lobe tumor removal, MAC and awake	Left anterior frontal lobe	Thin	No recording	Electrode fractured and recovered
	DBS implant, MAC and awake	Left dorsolateral prefrontal lobe	Thin	Short recording, but some fracture during recording	Electrode fractured and recovered
	DBS implant, MAC and awake	Left dorsolateral prefrontal lobe	Thick	Recording, but noise was significant	Electrode intact, noise considerable
	DBS implant, MAC and awake	Left dorsolateral prefrontal lobe	Thick	Recording, but noise was significant	Electrode intact, noise considerable
Pt. 01	DBS implant, generalized anesthesia, not awake	Right dorsolateral prefrontal lobe	Thick	262 total clusters, 202 single units, 60 MUA clusters	None, Electrode intact and recovered
Pt. 02	DBS implant, MAC and awake	Left dorsolateral prefrontal lobe	Thick	312 total clusters, 178 single units, 134 MUA clusters	None, Electrode intact and recovered
	left anterior temporal lobectomy, MAC and awake	Left anterior temporal lobe	Thick	Recording, but noise was significant	Electrode intact, but considerable noise
Pt. 03	left anterior temporal lobectomy, generalized anesthesia, not awake	Left anterior temporal lobe	Thick	29 total clusters, 19 single units, 10 MUA clusters	None, Electrode intact and recovered
	DBS implant, MAC and awake	Left dorsolateral prefrontal lobe	Thick	Recording, but noise was significant	Electrode intact, but considerable noise

a Steps which changed noise levels

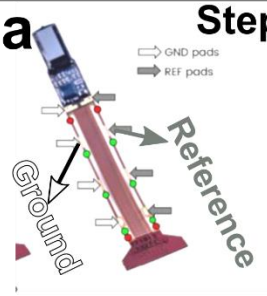

Degraded signal: We compared different ground and reference configurations. Noise levels were lower when the ground and reference were not tied together. (N=4)

Improved signal: Reference separated from ground decreased noise (N=5)

Improved signal: The best recordings included having a separate ground and reference wire, each with a single wire (MedTronic grounding wires) secured via TegaDerm to the side ground and reference pads on the electrode (N=3)

Ground and reference wire tied together

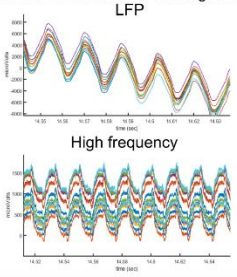

b Ground

Improved signal: BOVIE pad placed on the leg connected to the IMEC ground via a BNC cable to the NIDAQ PCI chassis BNC

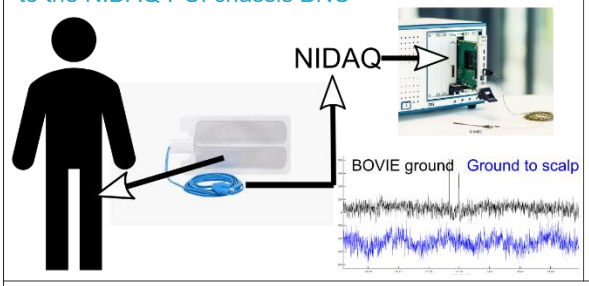

c Reference

Improved signal: Reference separated from ground and tied to a needle placed in the scalp or placed in CSF (N=4)

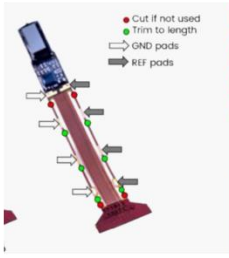

Degraded signal: Changing reference to internal reference (tip reference) increased 60 Hz and other noise (N=2)

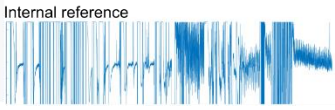

d Ground and Reference

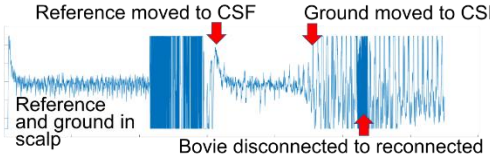

Improved signal: separate Ground and Reference via a needle in the scalp improved the signal (N=2)

Degraded signal: Grounding wire placed in CSF (not scalp)- caused LFP signal to saturate

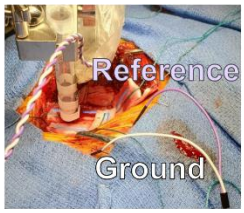

e External sources of noise

Improved signal: unplug the automated anesthesia IV pump from the wall with the machine on battery (N=4)

No change in signal: turning off OR lights, changing or turning off additional equipment other than the anesthesia machine

f Mechanical stabilization

Stabilization Option 1: securing the Neuropixels probe to three sterile cannulae attached to an AlphaOmega manipulator attached to the ROSA robot

Stabilization Option 2: securing the Neuropixels to a sterile syringe held by a sterile 3-axis manipulator on a Greenberg retractor

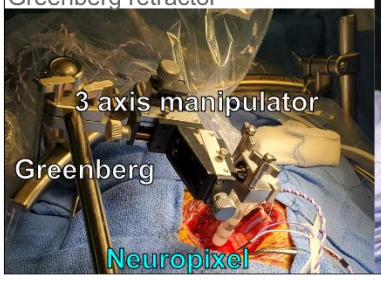

g Electrode Checks

Every electrode is tested for connections (in the OpenEphys or SpikeGLX software) and a quick saline test is done in the side sterile table.

Regular checks of the connections are done as the electrode is being moved into place in the sterile field. The electrode is also checked and photographed afterward for whether it is intact and connected.

Electrode intact after the recording

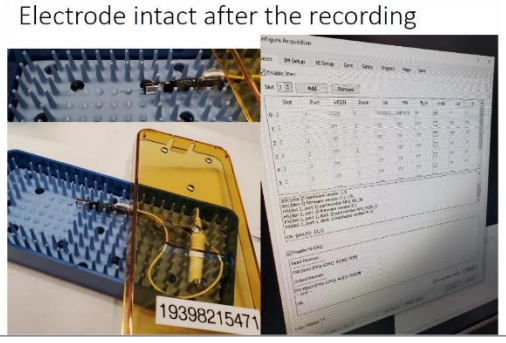

Supplemental Figure 1: Recording challenges and lessons learned. a. A major step in reducing noise levels was to separate the ground and reference, with a single separate wire going to the grounding pads on one side and another wire going to a grounding pad on the other side of the Neuropixels probe, pictured here. Securing the wires with Tegaderm improved the stability. Examples of considerable noise are shown in plots to the right. **b**. In two cases, 60 Hz noise was reduced by tying a ground to a spare BOVIE pad placed on the thigh of the patient under the sterile drape, as shown with the lower left LFP trace showing the signal grounded to the BOVIE versus grounded to a scalp needle electrode. **c**. We used the external reference tied to a sterile MedTronic grounding wire with a needle which, when placed in the scalp or CSF, improved the signal and reduced 60 Hz noise. We did test using the internal reference on the Neuropixels probe and found the noise increased significantly in the two cases we attempted the switch. **d**. The placement of the sterile ground and reference leads made a difference. Ground and reference in the scalp had an improved signal. Placing the ground (but not the reference) in the saline in the craniotomy caused the LFP signal to saturate and degraded the signal. **e**. Common 60 Hz noise and other noise decreased significantly if the anesthesia IV pump was unplugged from the wall and was run on battery during the recordings. Otherwise, turning off lights or other sources of noise (BOVIE cautery machine, AlphaOmega recording system, etc.) had no noticeable effect on noise. **f**. Mechanical stabilization of the probe involved two options, one using the ROSA robot combined with an AlphaOmega manipulator with the Neuropixels probe secured to cannulae. The second option involved using a 3-axis manipulator mounted on a Greenberg retractor over the craniotomy. **g**. Every Neuropixels probe is documented and checked several times during and after the procedure both via software and photographing the probes before, during, and afterward to determine if they are intact.

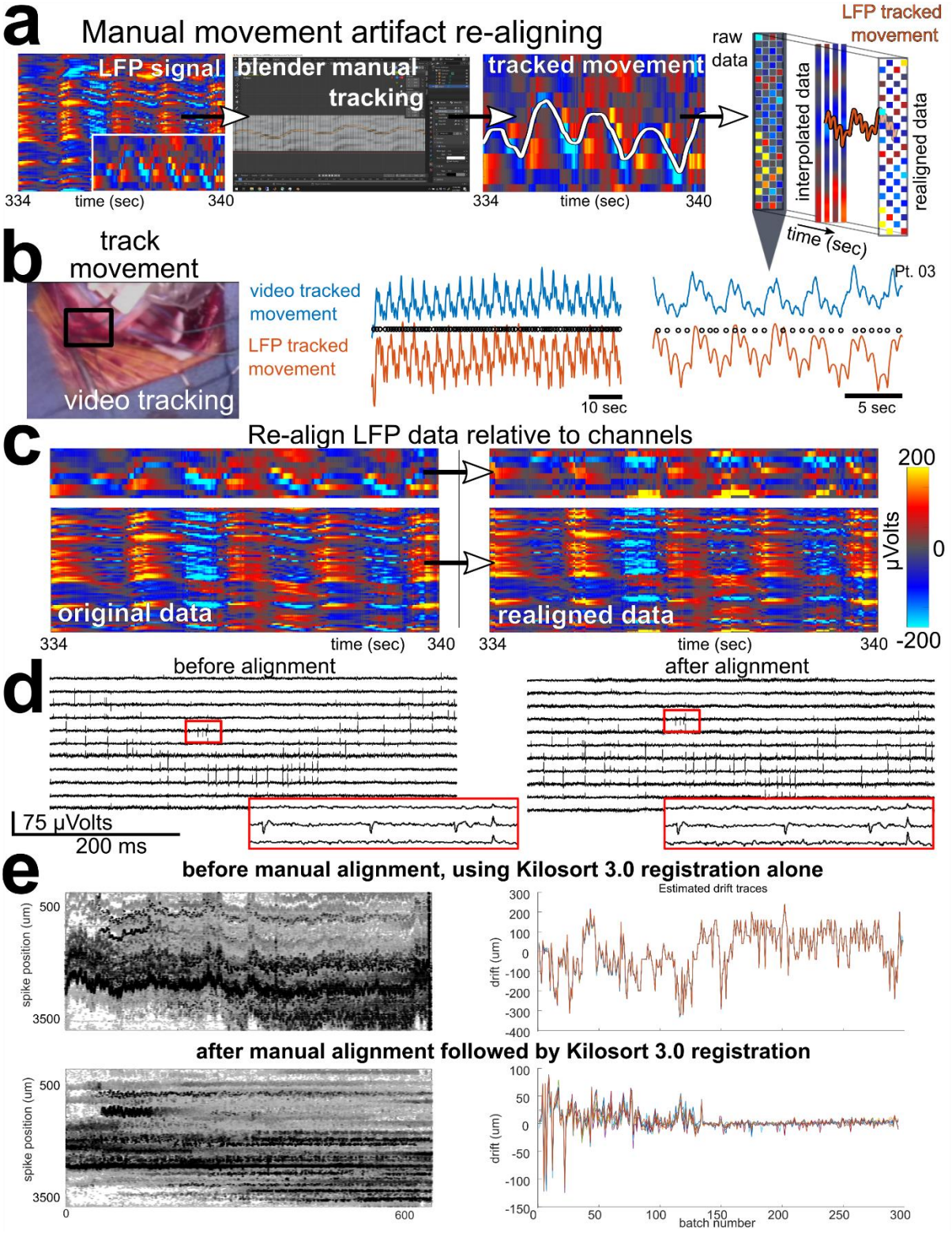

Supplemental Figure 2: Realigning the data relative to heartbeat-induced movement artifact. a. Illustration of evidence of tissue movement relative to the electrode recordings in the LFP (shown in red-blue color scale with the range in µvolts shown in **c**). This is quantified by

manually tracing these “band shifts” using the Blender program, followed by detection of these movements in the LFP and tracking of these movements across channels (white line, second to rightmost plot). **b.** Validation of movement being reflected in the LFP channel shifts. Left: video of the intraoperative recording and the pumping evident in the CSF surrounding the electrode was tracked through time. Right: Simultaneous traces of the video tracked movements and the LFP-tracked movements in the same patient (Pt. 03) at two different scales. Generally, the magnitude of the movement artifact was on the order of 80-100 μm. **c.** LFP before (left) and after (right) adjusting for movement effects. **d.** High frequency (action potential) frequency signal before (left) and after (right) adjusting for movement effects. **e**. Top row: Kilosort 3.0 registration and alignment alone could not compensate for the drift evident in the detected spike waveforms (left) and the estimated drift spanned hundreds of microns (right). Bottom row: manual alignment (a-b) followed by Kilosort 3.0 sorting resulted in improved spike alignment through time (left) and reduced drift (right).

Supplemental Figure 3. Example complex waveforms for six different units (each color-coded set of waveforms) across the data set. Original waveforms are overlaid relative to the recorded channels, with the grey bars to the right indicating the location of the units along the Neuropixels probe.

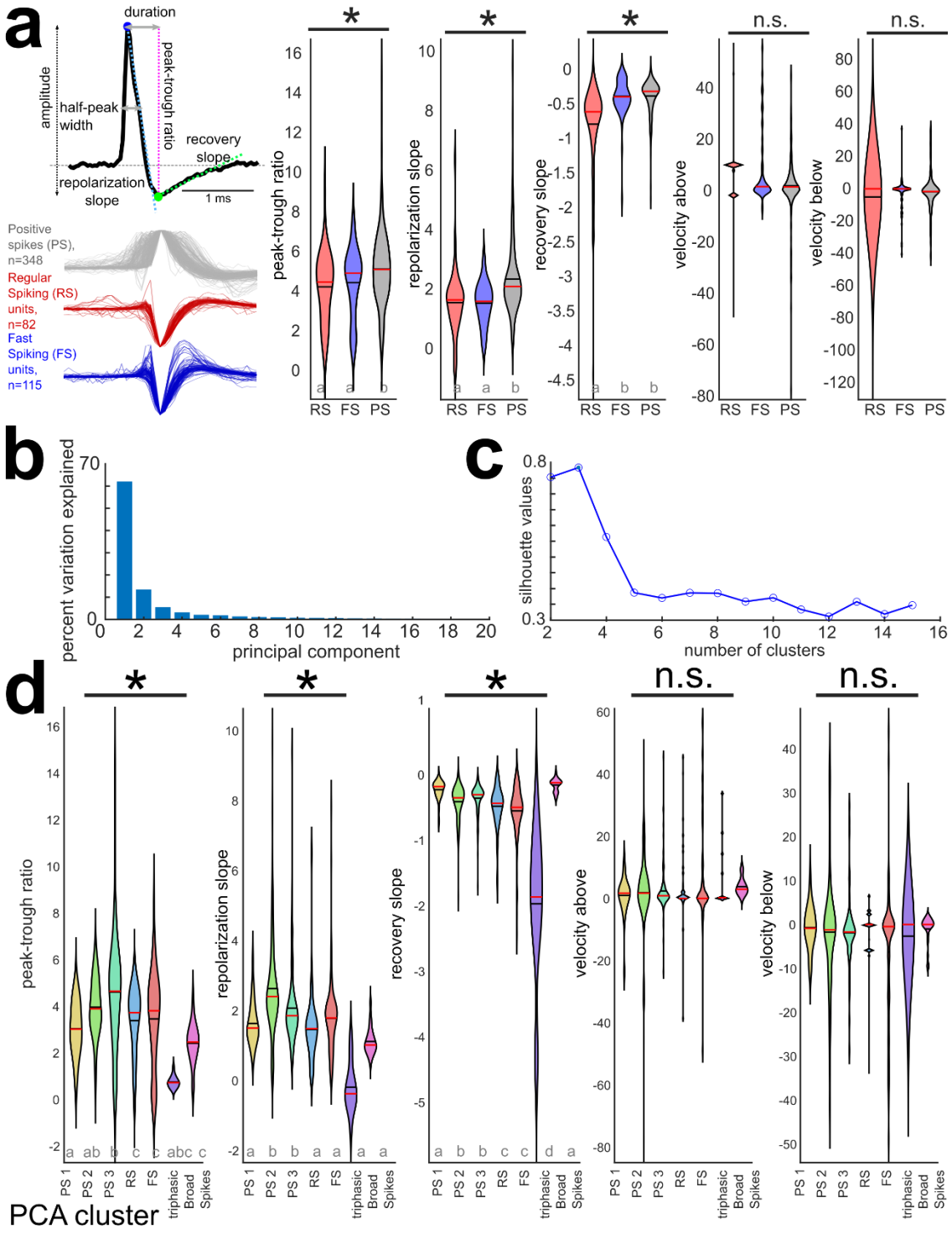

Supplemental Figure 4. Waveform measures and PCA with k-means clustering.

a. Waveforms per cluster color coded as RS, FS, or PS clusters using the "standard" grouping approach based on waveform duration [20]. The peak-trough ratio, repolarization slope, recovery slope, velocity above, and velocity below the center point (channel with the largest waveform)

violin plots are shown for the different waveform types. * indicate significant differences between all putative cell or waveform types, Kruskal-Wallis multiple comparison test, $p<0.001$ with *post hoc* Tukey-Kramer test. Grey letters a-c indicate statistically separable groups. **b**. Percent variance explained by each principal component calculated across the first 6 channels per unit. **c**. Silhouette values for each k-means cluster number for the first 40 principal components. **d**. The peak-trough ratio, repolarization slope, recovery slope, velocity above, and velocity below the center point (channel with the largest waveform) violin plots for the different clustered waveforms using PCA clustering.

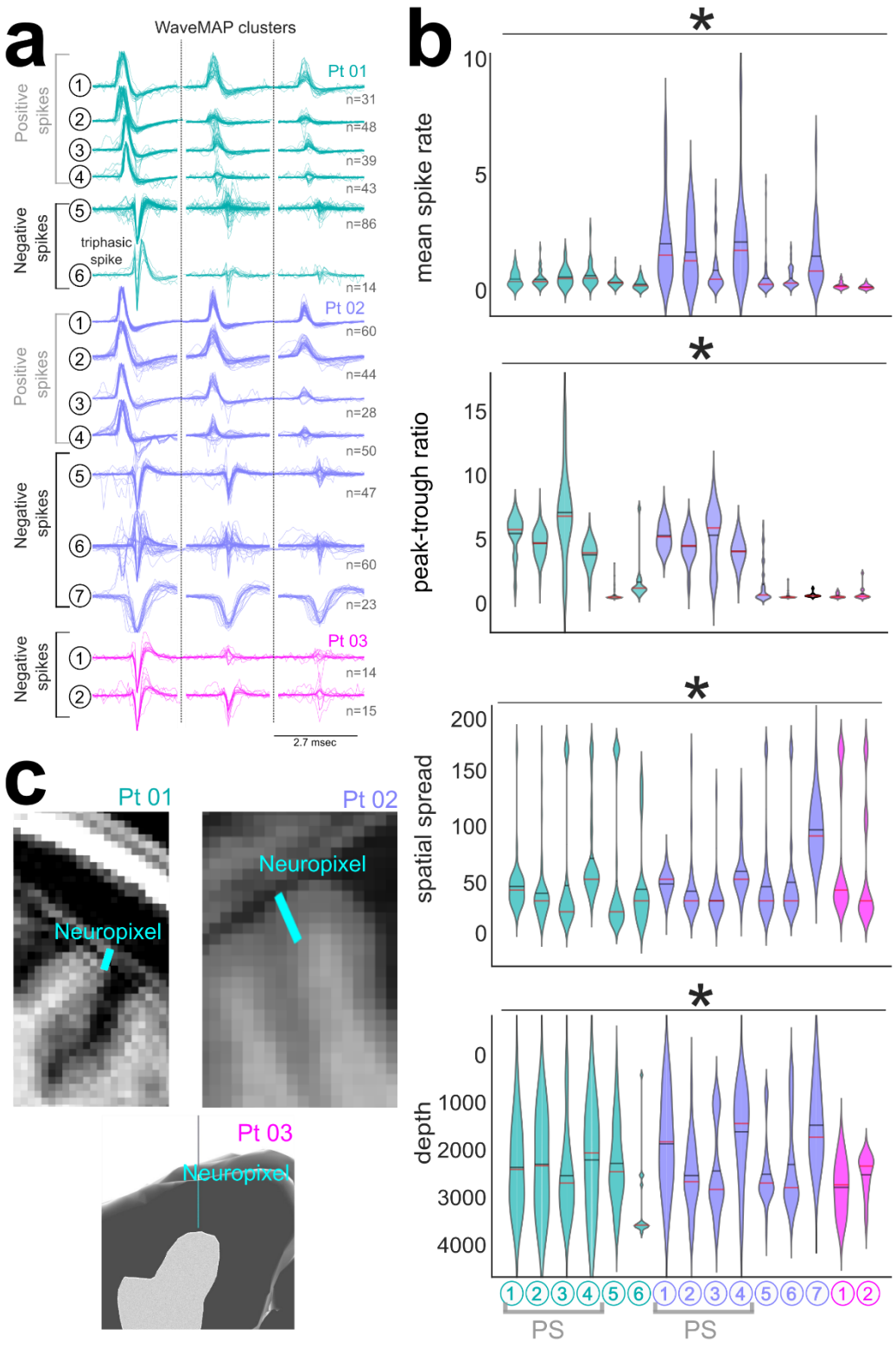

Supplemental Figure 5. Waveform Features of Units Clustered with WaveMAP.

a. Waveforms per cluster per patient (indicated as Pt. xx). The sorted clusters (with WaveMAP)

was performed on the per-patient level which is in contrast with the WaveMAP clustering performed across all three participants (Fig. 3). **b**. The remaining measures are per patient, showing mean firing rate, peak-trough ratio, spatial spread, and depth violin plots for the different clusters. * indicate significant differences between putative cell or waveform types, Kruskal-Wallis multiple comparison test, $p<0.001$. **c**. Electrode locations relative to the cortical surface and cortical regions.